Electronic Supplementary Material (ESI) for Journal of Materials Chemistry A.

Enhanced Hydrogen Evolution Efficiency Achieved by Atomically Controlled Platinum Deposited on Gold Nanodendrites with High-Index Surfaces

Ying-Huang Lai,[1]* Sin-Ren Li,[1#] Swathi M G,[1#] Hsiao-Tzu Chang,[1#] Yu-Bin Huang,[1] Yen-Ken Li,[1] Yu-Mei Chen,[1] Shivaraj B. Patil,[1] Shu-Yi Chang,[1] Po-Kai Chen,[1] Chia-Che Chang,[1] Yi-Chia Chen,[1] Chih-Wen Pao,[2] Jeng-Lung Chen,[2] Chuan-Yu Wei,[3] I-Kuan Lin,[3] Hung-Lung Chou,[4] Chun-Jen Su,[2] U-Ser Jeng,[2,5] Tsung-Rong Kuo,[6] Cheng-Yen Wen,[3,7,8] Di-Yan Wang[1]*

[1]Department of Chemistry, Tunghai University, Taichung 40704, Taiwan

[2] National Synchrotron Radiation Research Center, Hsinchu 30076, Taiwan

[3] Department of Materials Science and Engineering, National Taiwan University, Taipei 10617, Taiwan

[4] Graduate Institute of Applied Science and Technology, National Taiwan University of Science and Technology, Taipei 106, Taiwan

[5]Chemical Engineering Department, National Tsing-Hua University, Hsinchu, 30013, Taiwan

[6] Graduate Institute of Nanomedicine and Medical Engineering, College of Biomedical Engineering and International Ph.D. Program in Biomedical Engineering, College of Biomedical Engineering, Taipei Medical University, Taipei 11031, Taiwan

[7] Center of Atomic Initiative for New Materials, National Taiwan University, Taipei 10617, Taiwan

[8] International Graduate Program of Molecular Science and Technology, National Taiwan University, Taipei 10617, Taiwan

Corresponding authors: yhlai@go.thu.edu.tw and diyanwang@thu.edu.tw

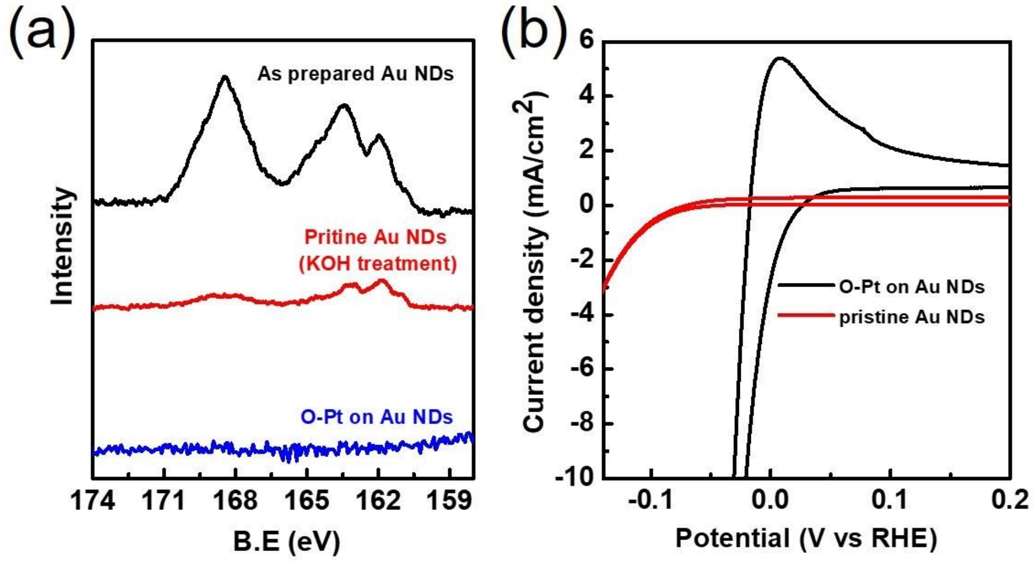

Figure S1. (a) XPS spectra of S 2p for the as-prepared Au NDs, Au NDs with KOH treatment (pristine Au NDs) and O-Pt on Au NDs. (b) CV results for pristine Au NDs and O-Pt on Au NDs in 0.5 M H_2SO_4 at a scan rate of 10 mV s^{-1}.

Figure S1a shows representative X-ray photoelectron spectroscopy (XPS) measurements regarding the spectral region of the S 2p level for the Au NDs at three different level that is, as-prepared Au NDs, pristine Au NDs, O-Pt on Au NDs. The results indicate that the peaks at lower binding energy (161.96 eV and 163.44 eV) and higher binding energy (168.48 eV) relate to the cysteine compound and sulphate compound present on the surface of as-prepared Au NDs, respectively. Simultaneously for the Au NDs with KOH treatment, those two peaks (161.96 eV & 163.44 eV) intensity become low and no sulphate compound was found. After Pt atom deposition, no signal of cysteine residue was found in O-Pt on Au NDs. According to the XPS analysis, the contamination on the surface of Au NDs can be efficiently removed. **Figure S1b.** shows CV studies to understand the electrochemical behavior of pristine Au NDs and O-Pt on Au NDs. All the measurements were performed in the potential window of -0.15 to 0.2 V (vs RHE) at sweep rate of 10 mV s^{-1} in the electrolyte of 0.5 M H_2SO_4. The results show that after Pt atom deposition, clear Pt-H desorption peak was found in the positive potential range but no obvious reduction peak of Pt oxide was found. These results will correlate with only small amount Pt atom deposited on the surface of Au NDs with clean high index facets.

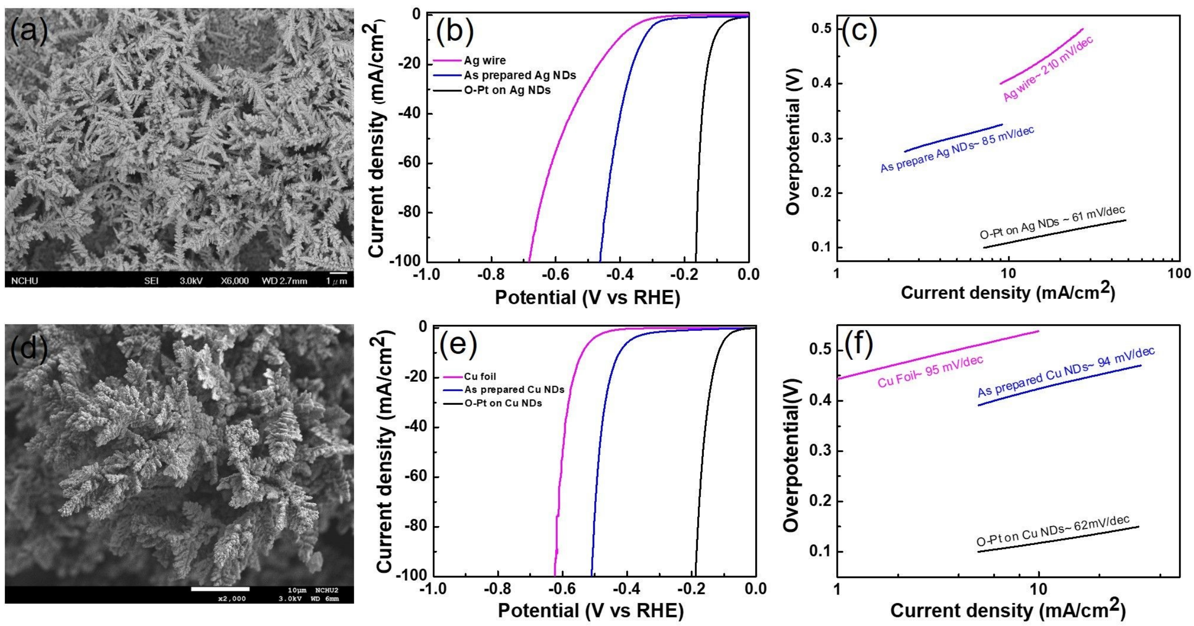

Figure S2. (a & d) SEM image of O-Pt on Ag NDs and O-Pt on Cu NDs respectively. (b & e) HER polarization curves of Ag wire, as prepared Ag NDs, O-Pt on Ag NDs and, Cu foil, as prepared Cu NDs, O-Pt on Cu NDs at a scan rate of 5 mV s^{-1} in 0.5 M H_2SO_4 solution respectively. (c & f) are the Tafel plots for Ag wire, as prepared Ag NDs, O-Pt on Ag NDs and, Cu foil, as prepared Cu NDs, O-Pt on Cu NDs respectively.

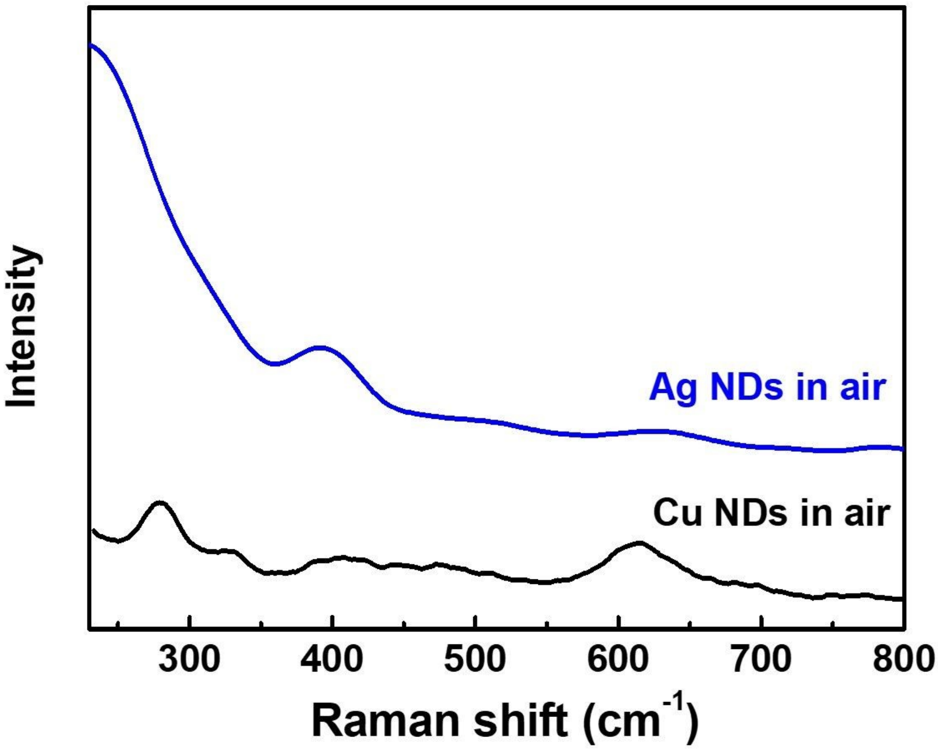

Figure S3. Raman spectra of Cu NDs and Ag NDs with exposure in air

Figure S3 shows Raman spectra of Cu NDs and Ag NDs with exposure in air. The results indicate that surface oxidation peak of Cu-O and Ag-O for Cu NDs and Ag NDs respectively. So, the less HER activity of Cu NDs and Ag NDs in comparison with O-Pt on Au NDs as showed in Figure S2 features the unstable surface structure on Cu and Ag, resulting in outcomes in less HER activity.

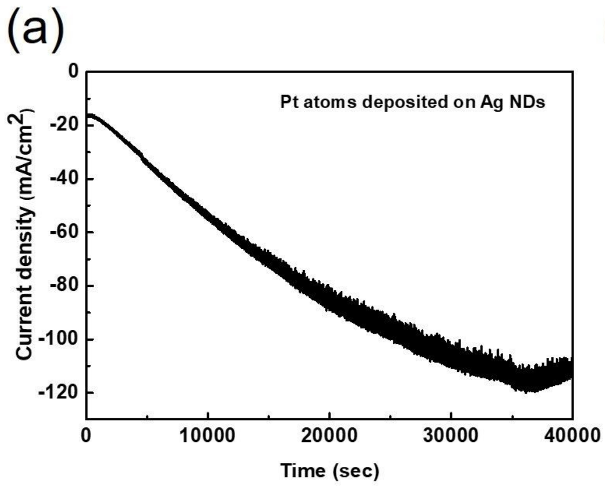

Figure S4. long term i-t curve of (a) Pt atoms deposited on Ag NDs and (b) Cu NDs with constant potential -0.35 V and -0.43 V (vs. RHE, without IR compensation) in 0.5 M H_2SO_4 solution, respectively.

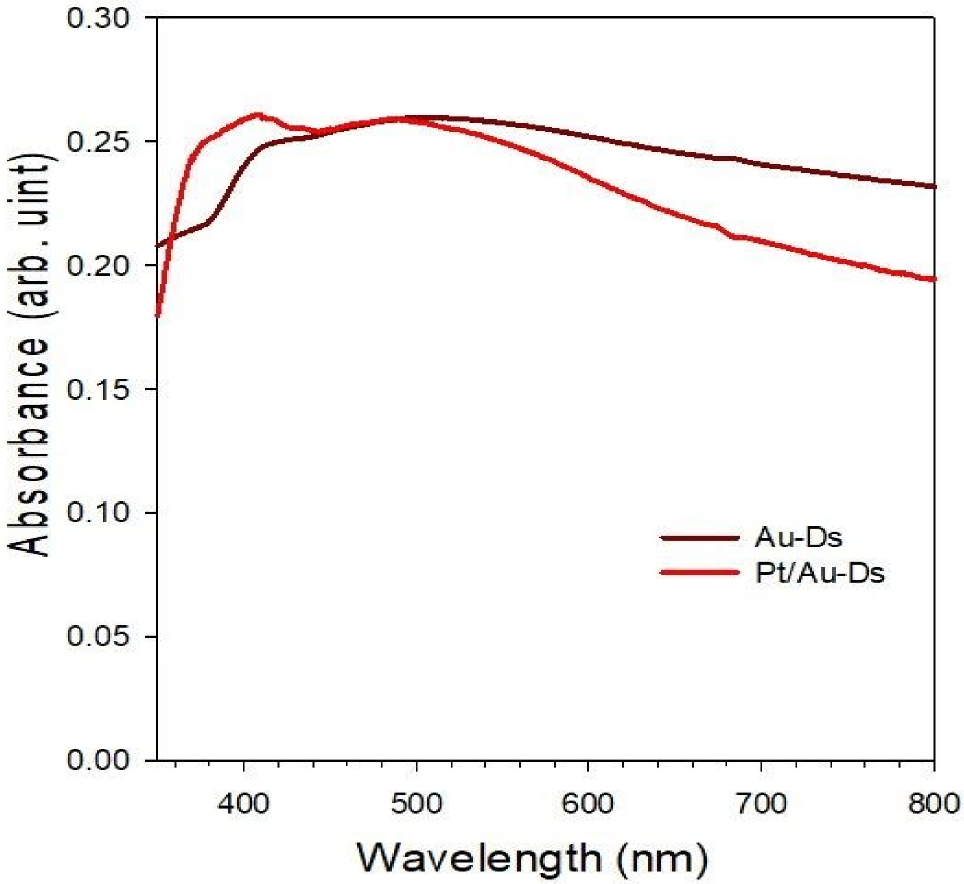

Figure S5. UV-Vis absorption spectra of Au NDs and O-Pt on Au NDs.

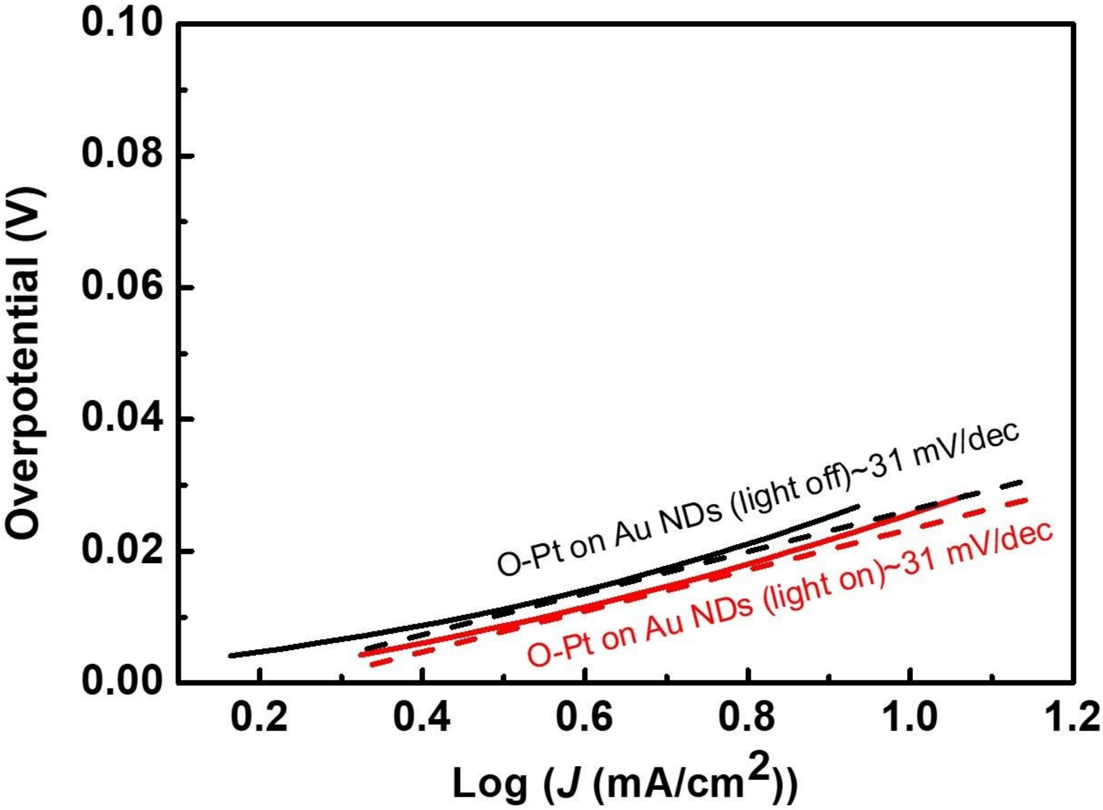

Figure S6. Tafel plots for O-Pt on Au NDs before and after light illumination in 0.5 M H_2SO_4

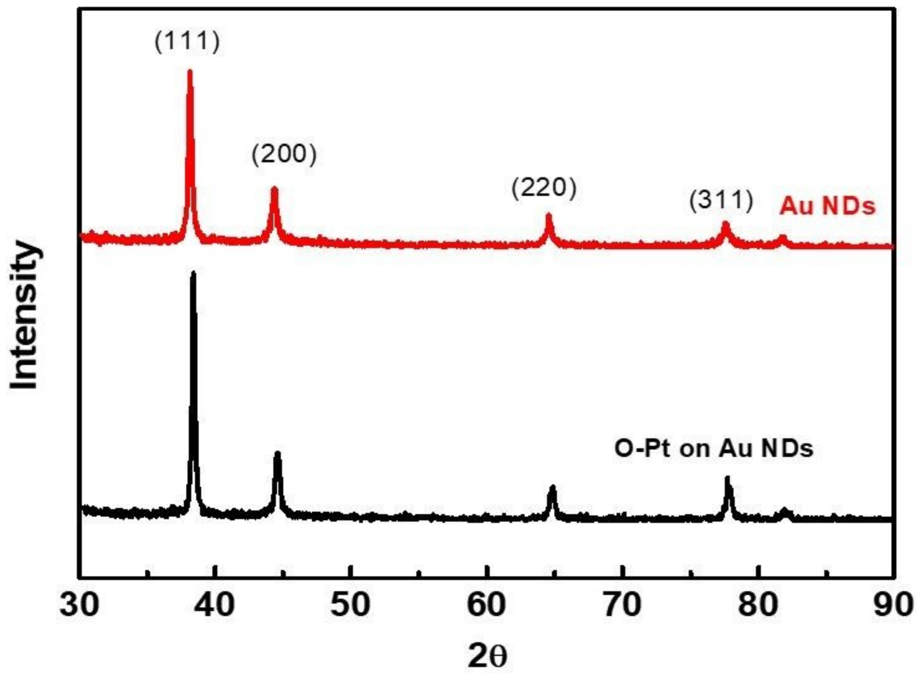

Figure S7. The XRD spectra of pristine Au NDs and O-Pt on Au NDs.

Figure S7 shows the XRD spectra of pristine Au NDs and O-Pt on Au NDs. All the peaks can be indexed to the Au (111), (200), (220), (311), crystal face without any additional peak observed. Therefore, it is difficult to distinguish the crystal phase of Pt and Au in O-Pt on Au NDs, because Pt is too few to be detected by XRD measurement.

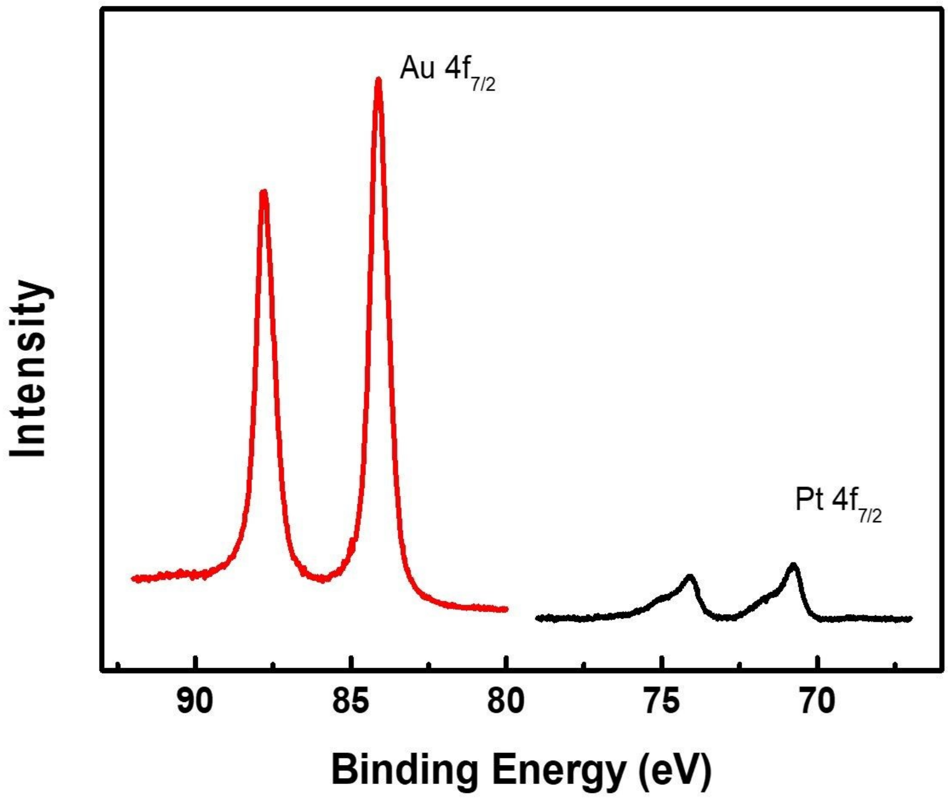

Figure S8. XPS spectra of O-Pt on Au NDs after HER stability test.

Figure S8. Shows the XPS spectra of O-Pt on Au NDs after HER stability test. Here, we found that Pt and Au signal of the catalysts after HER stability still can be observed. It indicated that our catalysts exhibited a good stability on HER for a long time.

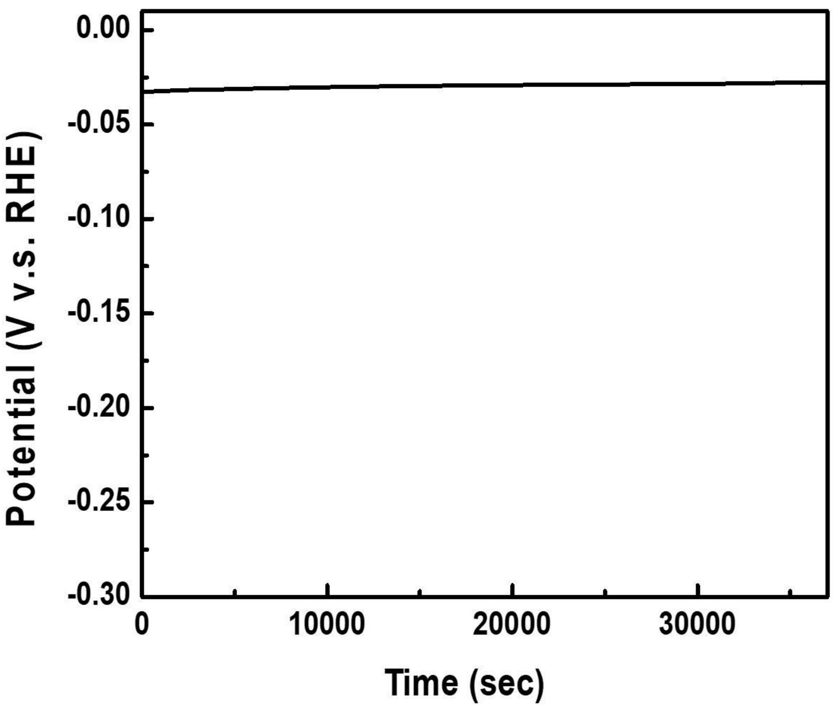

Figure S9. Chronopotentiometry (CP) plot of the catalysts with applying a constant current of 20 mA/cm^2 for 10 hours.

Table S1. Pt loading amount on Au NDs analyzed by ICPMS

Catalysts	Pt loading amount (% versus Au)
F-Pt on Au NDs	0.061%
O-Pt on Au NDs	0.19%
E-Pt on Au NDs	0.51%

Table S2. Comparative table for the presence of Pt content with TOF values @ certain overpotential modified with different materials on different substrate.

Sample	Substrate	Pt content	Overpotential mV	TOF value H_2 s^{-1}	Reference
O-Pt on Au NDs	Carbon fiber paper (CFP)	5.5 % (on surface) 0.19 wt%	50	40.1	**Present work**
PtW NPs	RDE	16 wt%	-	-	[1]
Pt_1/OLC	Pt mesh	0.27 wt%	100	40.78	[2]
Ni-MOF @Pt	Glassy carbon (GC)	0.04 (mg/cm^2)	-	-	[3]
Pt GT-1	GC	0.5 wt%	18	7.22	[4]
Pt/GNs	GC	14.7 wt%	-30	0.854	[5]
A-Ni@ DG	GC	-	100	5.7	[6]
Pt GDY_2	Ti foil	4.6 ($\mu g/cm^2$)	-	-	[7]
Pt_2 Pd/N-graphene	GC	0.118 (mg/cm^2)	-	-	[8]
Pt NPs/2D Ni $(OH)_2$	GC	0.001 (mg/cm^2)	-	-	[9]
Pt/vertical graphene Nanosheet arrays	Carbon cloth (CC)	0.042 (mg/cm^2)	-	-	[10]
Pt NC/N-graphene	GC	5.0 wt%	24	2.05	[11]
$Ru/C_3N_4/C$	GC	-	100	4.2	[12]
ALD50Pt/NGNs	GC	2.1 wt%	-	-	[13]
PtPs@MoS_2@graphene	Nickel woven fabrics (NiWF)	5.38 wt%	-	-	[14]

Pt nanocuboids/rGO	GC	0.078 (mg/cm^2)	-	-	[15]
Pt NWs/SL-Ni (OH)$_2$	GC	0.04 (mg/cm^2)	-	-	[16]

Table S3. Comparative table for the HER performance of the recently reported catalyst.

sample	Loading amount	Current density $mA\ cm^{-2}$	Overpotential (η) mV	Reference
O-Pt on Au NDs	3.8 μg Pt cm^{-2}	10	~18	**Present work**
PtW NPs	20.3 μg Pt cm^{-2}	10	19.4	[1]
Pt_1/OLC	510 μg cm^{-2}	10	38	[2]
Ni-MOF @Pt	0.2 mg cm^{-2}	10	43	[3]
Pt GT-1	0.28 mg cm^{-2}	10	18	[4]
Pt/GNs	0.099 mg cm^{-2}	10	-25	[5]
Pt GDY_2	-	10 A/mg	67.1	[7]
Pt_2 Pd/N-graphene	0.159 mg cm^{-2}	10	58	[8]
Pt NPs/2D Ni $(OH)_2$	0.011 mg cm^{-2}	5	123	[9]
Pt/vertical graphene Nanosheet arrays	-	10	60	[10]
Pt NC/N- graphene	0.113 mg cm^{-2}	10	24	[11]
ALD50Pt/NGNs	0.076 mg cm^{-2}	16	50	[13]
PtPs@MoS_2@graphene	-	10	56	[14]
Pt nanocuboids/rGO	0.170 mg cm^{-2}	10	~75	[15]
Pt NWs/SL-Ni $(OH)_2$	0.016 mg cm^{-2}	4	86	[16]
AuPtNDs	6 μg cm^{-2}	10	50	[17]

References:

(1) Kobayashi, D.; Kobayashi, H.; Wu, D.; Okazoe, S.; Kusada, K.; Yamamoto, T.; Toriyama, T.; Matsumura, S.; Kawaguchi, S.; Kubota, Y. Significant Enhancement of Hydrogen Evolution Reaction Activity by Negatively Charged Pt through Light Doping of W. *Journal of the American Chemical Society* **2020,** *142* (41), 17250.

(2) Liu, D.; Li, X.; Chen, S.; Yan, H.; Wang, C.; Wu, C.; Haleem, Y. A.; Duan, S.; Lu, J.; Ge, B. Atomically dispersed platinum supported on curved carbon supports for efficient electrocatalytic hydrogen evolution. *Nature Energy* **2019,** *4* (6), 512.

(3) Rui, K.; Zhao, G.; Lao, M.; Cui, P.; Zheng, X.; Zheng, X.; Zhu, J.; Huang, W.; Dou, S. X.; Sun, W. Direct hybridization of noble metal nanostructures on 2D metal–organic framework nanosheets to catalyze hydrogen evolution. *Nano Letters* **2019,** *19* (12), 8447.

(4) Tiwari, J. N.; Sultan, S.; Myung, C. W.; Yoon, T.; Li, N.; Ha, M.; Harzandi, A. M.; Park, H. J.; Kim, D. Y.; Chandrasekaran, S. S. Multicomponent electrocatalyst with ultralow Pt loading and high hydrogen evolution activity. *Nature Energy* **2018,** *3* (9), 773.

(5) Yan, X.; Li, H.; Sun, J.; Liu, P.; Zhang, H.; Xu, B.; Guo, J. Pt nanoparticles decorated high-defective graphene nanospheres as highly efficient catalysts for the hydrogen evolution reaction. *Carbon* **2018,** *137*, 405.

(6) Zhang, L.; Jia, Y.; Gao, G.; Yan, X.; Chen, N.; Chen, J.; Soo, M. T.; Wood, B.; Yang, D.; Du, A. Graphene defects trap atomic Ni species for hydrogen and oxygen evolution reactions. *Chem* **2018,** *4* (2), 285.

(7) Yin, X. P.; Wang, H. J.; Tang, S. F.; Lu, X. L.; Shu, M.; Si, R.; Lu, T. B. Engineering the coordination environment of single-atom platinum anchored on graphdiyne for optimizing electrocatalytic hydrogen evolution. *Angewandte Chemie International Edition* **2018,** *57* (30), 9382.

(8) Zhong, X.; Qin, Y.; Chen, X.; Xu, W.; Zhuang, G.; Li, X.; Wang, J. PtPd alloy embedded in nitrogen-rich graphene nanopores: high-performance bifunctional electrocatalysts for hydrogen evolution and oxygen reduction. *Carbon* **2017,** *114*, 740.

(9) Wang, L.; Zhu, Y.; Zeng, Z.; Lin, C.; Giroux, M.; Jiang, L.; Han, Y.; Greeley, J.; Wang, C.; Jin, J. Platinum-nickel hydroxide nanocomposites for electrocatalytic reduction of water. *Nano energy* **2017,** *31*, 456.

(10) Zhang, H.; Ren, W.; Guan, C.; Cheng, C. Pt decorated 3D vertical graphene nanosheet arrays for efficient methanol oxidation and hydrogen evolution reactions. *Journal of Materials Chemistry A* **2017,** *5* (41), 22004.

(11) Jiang, B.; Liao, F.; Sun, Y.; Cheng, Y.; Shao, M. Pt nanocrystals on nitrogen-doped graphene for the hydrogen evolution reaction using Si nanowires as a sacrificial template. *Nanoscale* **2017,** *9* (28), 10138.

(12) Zheng, Y.; Jiao, Y.; Zhu, Y.; Li, L. H.; Han, Y.; Chen, Y.; Jaroniec, M.; Qiao, S.-Z. High electrocatalytic hydrogen evolution activity of an anomalous ruthenium catalyst. *Journal of the American Chemical Society* **2016,** *138* (49), 16174.

(13) Cheng, N.; Stambula, S.; Wang, D.; Banis, M. N.; Liu, J.; Riese, A.; Xiao, B.; Li, R.; Sham, T.-K.; Liu, L.-M. Platinum single-atom and cluster catalysis of the hydrogen evolution reaction. *Nature communications* **2016,** *7* (1), 1.

(14) Li, X.; Zhang, L.; Zang, X.; Li, X.; Zhu, H. Photo-promoted platinum nanoparticles decorated MoS2@ graphene woven fabric catalyst for efficient hydrogen generation. *ACS applied materials & interfaces* **2016,** *8* (17), 10866.

(15) Xu, G.-R.; Hui, J.-J.; Huang, T.; Chen, Y.; Lee, J.-M. Platinum nanocuboids supported on reduced graphene oxide as efficient electrocatalyst for the hydrogen evolution reaction. *Journal of Power Sources* **2015,** *285*, 393.

(16) Yin, H.; Zhao, S.; Zhao, K.; Muqsit, A.; Tang, H.; Chang, L.; Zhao, H.; Gao, Y.; Tang, Z. Ultrathin platinum nanowires grown on single-layered nickel hydroxide with high hydrogen evolution activity. *Nature communications* **2015,** *6* (1), 1.

(17) Weng, X.; Liu, Y.; Wang, K.-K.; Feng, J.-J.; Yuan, J.; Wang, A.-J.; Xu, Q.-Q. Single-step aqueous synthesis of AuPt alloy nanodendrites with superior electrocatalytic activity for oxygen reduction and hydrogen evolution reaction. *International Journal of Hydrogen Energy* **2016,** *41* (40), 18193.